Proceedings of IMECE2005
2005 ASME International Mechanical Engineering Congress and Exposition
November 5-11, 2005, Orlando, Florida USA

IMECE2005-81122

ADHESION ENERGY OF SINGLE WALL CARBON NANOTUBE-POLYETHYLENE COMPOSITE: EFFECT OF MAGNETIC FIELD

M.S. Al-Haik,
School of Computational Science, Florida State University Tallahassee, FL 32306-4120
alhaik@csit.fsu.edu,

M.Y. Hussaini
School of Computational Science, Florida State University Tallahassee, FL 32306-4120
myh@csit.fsu.edu

H. Garmestani
School of Materials Science and Engineering, Georgia Institute of Technology
Atlanta, GA 30332-0245
hamid.garmestani@mse.gatech.edu

ABSTRACT

In this paper, we investigate the adhesion energy at the interface between single wall carbon nanotubes and polyethylene matrix with and without an external magnetic field. The carbon nanotubes are of two different chiralities -- armchair (10,10), and zigzag (10,0), and the external high magnetic field is of 25 Tesla intensity. The study employs molecular dynamics simulations and concludes that the magnetic field decreases the interfacial adhesion energy although it increases the individual potential energies of the nanotubes, the polyethylene, and the composite.

Keywords: Molecular dynamics, chirality, velocity-Verlet, OPLSAA force field.

INTRODUCTION

Owing to their exceptional mechanical properties (Young's modulus and tensile strength as high as 1 TPa and 200 GPa, respectively), high aspect ratio, and low density, carbon nanotubes (SWCNT) are promising reinforcements for polymer composites [1]. However, the effective utilization of SWCNT in composite applications depends strongly on the ability to disperse the nanotubes homogeneously throughout the polymer matrix without destroying the integrity of the nanotubes. In earlier investigations [2-3], the authors have employed high magnetic field to successfully disperse carbon nanotubes in a polymeric matrix while maintaining their structural integrity. Beside homogeneous dispersion, good interfacial bonding is required to achieve load transfer across the SWCNT-polymer interface [4]. Due to difficulties in devising experiments to study the SWCNT-polymer interface, molecular dynamics (MD) simulations have become increasingly popular in the investigations of reinforcement mechanisms in SWCNT-polymer composite systems. Molecular dynamics simulations of nanocomposite systems have been investigated by Wei et al. [5], Liao and Li [6], Frankland et al. [7], Frankland and Harik [8], and Al-Haik et al. [9], to cite a few. While most of these investigations consider MD simulations for nanotubes of different lengths with different types of polymers, to the best of our knowledge, only the study of Al-Haik et al. [9] investigates the effect of nanotube geometry (chirality) on the adhesion properties. They observe that substantial adhesion exists between the nanotube and the polyethylene when the nanotube has a low chiral index or smaller chiral angle (relatively long) in conformity with the composite principle that high aspect-ratio fibers yield stronger adhesion with the matrix. The focus of the present study is the effect of high magnetic field on adhesion energy of the polyethylene matrix and SWCNT of zigzag and armchair types. Assuming that there is no chemical bonding between the carbon nanotube and the polyethylene matrix after mixing, the system can be investigated for nonbonded interactions constituting the adhesion energy. This assumption was validated experimentally by Chang et al. [10],

for a system of SWCNT and polypyrole matrix using Raman scattering and X-ray diffraction.

For the sake of completeness, we start with a brief description of chirality of SWCNT, molecular dynamics, potential energy function and the solution algorithm. It is followed by a description of numerical experiments and discussion of results.

Chirality of carbon nanotubes

A single wall carbon nanotube (SWCNT) is characterized by it chiral vector = n + , which is denoted by (n, m), Fig. 1. It means it takes n times and m times on the honeycomb lattice sheet to reach the point (n, m) from the origin and roll up the sheet so that these two points coincide [11]. It is also common to identify a SWCNT by its tube diameter Dn, and chiral angle θ, which are uniquely determined by the integer pair (n, m):

$$\theta = \arctan\left(\frac{\sqrt{3}m}{2n+m}\right), \quad (1)$$

$$D_n = \frac{\sqrt{3}}{\pi} b\sqrt{\left(n^2 + m^2 + nm\right)}, \ (0 \le m \le n) \quad (2)$$

where b is the C–C bond length (0.142 nm). The chiral angle is the smallest angle between the circumference line (chiral vector) and the primitive lattice vector (zigzag direction) on the hexagonal sheet as shown in Fig.1.

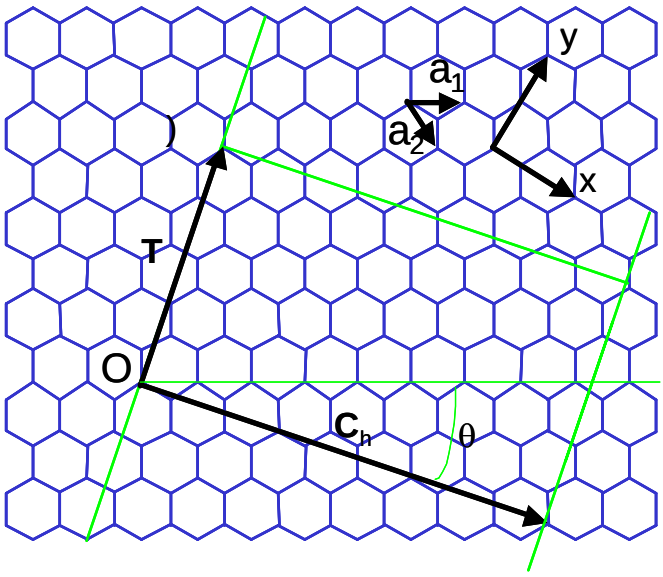

Fig. 1. Definition of chiral angle and chiral vector**.**

The nanotube configurations where the chiral angles have the values of 0o and 30o are the limiting cases referred to as "zigzag" and "armchair" respectively.

In terms of the chiral vector, the zigzag nanotube is defined as (n, 0) and the armchair nanotube as (n, n). The chiral angle q may be viewed as a measure of the twist in the tube, and this chirality has significant influence on the nanotube diameter. The thermal [12], electronic [13], and mechanical [14] properties of SWCNT vary substantially depending on the SWCNT diameters and chiral angles.

Molecular Dynamics, Potential Energy Function, And Adhesion Energy

In molecular dynamics, the classical equations of motion for an assembly of N interacting particles

$$m_i \frac{d\mathbf{v}_i}{dt} = \mathbf{F}_i = -\nabla_{\mathbf{r}i} E(\mathrm{r}_1, \mathrm{r}_2, ..., \mathrm{r}_N) \quad (3)$$

are solved, where mi is the atomic mass of the i-th atom, $\mathbf{r}_i$ and $\mathbf{v}_i$ are the position and velocities of the particles relative to a reference coordinate system. F is the total force acting on the ith particle and E (r_1, r_2, r_N) is E the potential energy of the system. These equations are integrated using the velocity Verlet (VV) finite difference method [15], which yields the positions, velocities and accelerations of the particles in the system as a function of time -- **r** (t), **v** (t), and **a** (t) respectively. The velocity Verlet discretization can be written as, [15]

$$\begin{aligned} \mathbf{r}(t+\delta t) &= \mathbf{r}(t) + \delta t \mathbf{v}(t) + \frac{1}{2}(\delta t)^2 \mathbf{a}(t) + O((\delta t)^3) \\ \mathbf{a}(t+\delta t) &= \mathbf{a}(r_1(t+\delta t), ... r_N(t+\delta t); t+\delta t) \\ \mathbf{v}(t+\delta t) &= \mathbf{v}(t) + \frac{1}{2}\delta t \mathbf{a}\left[a(t) + \mathbf{a}(t+\delta t)\right] + O((\delta t)^3) \end{aligned} \quad (4)$$

This algorithm is second-order accurate, time reversal invariant, allows local time stepping, and requires only one evaluation of the acceleration per time step.

The potential energy function employed in this investigation is known as OPLSAA (optimized potentials for liquid simulations-all atoms) that includes harmonic bond-stretching and angle-bending terms, a Fourier series for torsional energetics, and Coulomb and Lennard-Jones terms for the nonbonded interactions [16]:

$$E_{bond} = \sum_i k_{b,i}\left(r_i - r_{o,i}\right)^2, \quad (5)$$

$$E_{angle} = \sum_i k_{\vartheta,i}\left(\vartheta_i - \vartheta_{o,i}\right)^2, \quad (6)$$

$$E_{torsion} = \sum_i \left[\begin{array}{l} \frac{1}{2} V_{1,i}\left(1+\cos\varphi_i\right) + \frac{1}{2} V_{2,i}\left(1-\cos 2\varphi_i\right) + \\ \frac{1}{2} V_{3,i}\left(1+\cos 3\varphi_i\right) \end{array} \right], \quad (7)$$

$$E_{non-bonded} = \sum_i \sum_{j>i} \left\{ \begin{array}{l} \frac{q_i q_j e^2}{r_{ij}} + \\ 4\varepsilon_{ij}\left[\left(\frac{\sigma_{ij}}{r_{ij}}\right)^{12} - \left(\frac{\sigma_{ij}}{r_{ij}}\right)^{6}\right] \end{array} \right\} \quad (8)$$

Here, k_b and k_J are the force constants, the r_0 and J_0 the initial bond lengths and angles respectively, V the Fourier coefficients, q the partial atomic charges, and s and e the Lennard-Jones radii and well-depths respectively. The nonbonded interactions are evaluated intermolecularly and for intramolecular atom pairs separated by three or more bonds. OPLSAA was parameterized, tested, and validated for hydrocarbons [17-19].

The adhesion energy is estimated as the difference between the potential energy of the composite system and the potential energies for the polyethylene and the corresponding SWCNT:

$$\Delta E = E_{Total} - (E_{SWCNT} + E_{PE}) \quad (9)$$

where E_{Total} is the total potential energy of the composite at the end of MD equilibration, E_{SWCNT} is the energy of the nanotube alone, and E_{PE} is the energy of the polymer alone.

Magnetic Field and Molecular Dynamics

The idea of introducing an external force field in the molecular dynamics simulations of polymeric materials is not new. For example, Weber and Annan [20] introduced external compression and shearing forces in their adiabatic molecular dynamics (MD) simulation of ethane molecules to examine the alignment of the molecules in the direction of the shearing field. Tian et al [21] incorporated an applied electric field in their MD simulations of the switching dynamics of nematics liquid crystals with positive polarity anisotropy. In the present study, we represent a system of polyethylene-single wall carbon nanotube as a system of charged particles subject to an external static homogeneous magnetic field. The explicit time stepping in a conventional MD simulation of such a system is restricted by the smaller of the two time scales

-- Larmor time-scale and characteristic time of the internal interactions of the system. In a high magnetic field, which is the context of the present study, the Larmor time-scale is very much smaller than that of the internal interactions, and therefore the MD simulation becomes prohibitively expensive. Here, we employ the algorithm due to Spreiter and Walter [22], which relaxes the Larmor restriction while maintaining the overall accuracy of the discretization scheme. For the sake of completeness, we provide a brief description of the algorithm.

A particle with specific charge qi/mi performs Larmor oscillations of frequency $\omega_i = q_i B/m_i$ when influenced by a magnetic field B. With a homogeneous magnetic field B=(0, 0, B) along the z-axis, the acceleration of each particle is given by

$$\mathbf{a}_i(t) = \mathbf{a}_i^C(t) - \omega \mathbf{e}_z \times \mathbf{v}_i(t) \quad (10)$$

where $\boldsymbol{a}_i^c(t) = \boldsymbol{a}^C(r_{1i}(t),....., r_{Ni}(t); t)$ is the part of acceleration which does not depend on velocities, and $\mathbf{e}_z$ is the unit vector along the z direction. Introducing this term in the velocity Verlet algorithm[21] the equations of motion update the particle positions

$$r_x(t+\delta t) = r_x(t) + \frac{1}{\omega}\left[v_x(t)\sin(\omega\delta t) - v_y(t)C(\omega\delta t)\right] + \frac{1}{\omega^2}\left[-a_x^c(t)C(\omega\delta t) - a_y^c(t)S(\omega\delta t)\right] + O((\delta t)^3), \quad (11)$$

$$r_y(t+\delta t) = \text{like } r_x(t+\delta t), \text{ exchange } x \leftrightarrow y, \omega \leftrightarrow -\omega,$$

$$r_z(t+\delta t) = r_z(t) + \delta t v_z(t) + \frac{1}{2}(\delta t)^2 a_z^c(t) + O((\delta t)^3),$$

where $S(\omega\delta t)=\sin(\omega\delta t)-\omega\delta t$, $C(\omega\delta t)=\cos(\omega\delta t)-1$. The acceleration of the particles at $(t+\delta t)$ is obtained from Eq. (3), while the particle velocity is obtained from

$$v_x(t+\delta t) = v_x(t)\cos(\omega\delta t) + v_y(t)\sin(\omega\delta t) + \frac{1}{\omega}\left[-a_y^c(t)C(\omega\delta t) + a_x^c\sin(\omega\delta t)\right] + \frac{1}{\omega^2}\left[\begin{array}{l} -\frac{a_x^c(t+\delta t) - a_x^c(t)}{\delta t} C(\omega\delta t) - \\ \frac{a_y^c(t+\delta t) - a_y^c(t)}{\delta t} S(\omega\delta t) \end{array}\right] + O((\delta t)^3) \quad (12)$$

$$v_y(t+\delta t) = \text{like } v_x(t+\delta t), \text{ exchange } x \leftrightarrow y, \omega \leftrightarrow -\omega$$

$$v_z(t+\delta t) = v_z(t) + \frac{1}{2}\delta t\left[a_z^c(t) + a_z^c(t+\delta t)\right] + O((\delta t)^3)$$

Note that the time step δt is independent of the Larmor time scale $2\pi/\omega$, and it only needs to resolve the characteristic time scale of internal physical interactions. Thus, the Spreiter and Walter version of the velocity Verlet algorithm enlarges the domain of MD applications to include strong external magnetic forces.

NUMERICAL EXPERIMENTS

All of the MD simulations are performed within the framework of the NPT (isothermal-isobaric) statistical ensemble for a periodic system, which is characterized, by a fixed number of atoms N, constant pressure P = 1 atm, and constant temperature T = 300 K. First, the NPT ensemble allows the molecular dynamics simulation for systems with relatively small number of particles (1000 atom) by calculating the trajectories in various ways. Second, it simulates the effect of surrounding particles without creating undesirable surfaces. Third, this

method simulates both the forces that drive the system to equilibrium at a given temperature and pressure, and the forces that cause the energy and volume of the system to fluctuate about their equilibrium values [23]. Nose-Hoover extended system thermostat is used for the temperature control and the Berendsen method is used to maintain the desired constant pressure in the periodic box.

The simulations are carried out using TINKER©; a package of molecular dynamics simulation subroutines [24]. The simulations terminate if the variation of the potential energy is in the prescribed range of 0.0001-0.001 (when equilibrium can be assumed). All of the simulations stop at 10 pico seconds. The integration time step δt= 1.0 fs, and the cutoff distance for the 12--6 Lennard--Jones potential is 1.05 nm.

Single wall carbon nanotubes of two different chiral types, zigzag (10,0) and armchair (10,10), and a single polyethylene chain are constructed separately. The unrelaxed chemical structures of the three different materials utilized in this investigation are shown in Fig. 2. While these nanotubes have different diameters and lengths, they all consist of 600 carbon atoms each. Hydrogen atoms are added to the open ends of the carbon nanotubes to eliminate the unsaturated boundary effect. The exact numbers of carbon and hydrogen atoms for the SWCNT and the polyethylene are presented in Table 1.

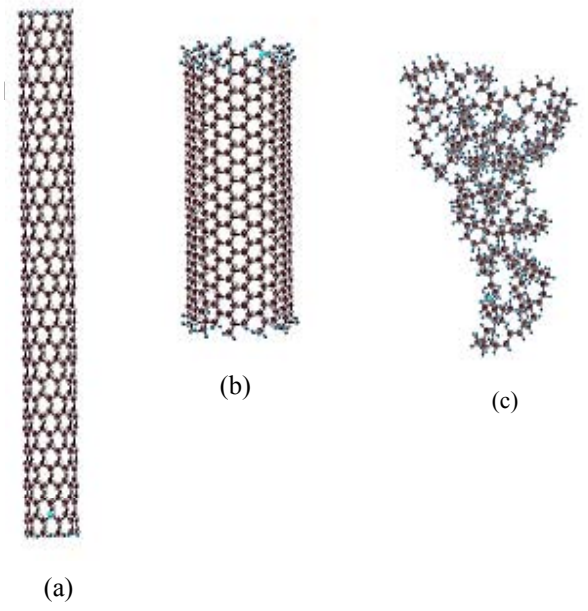

Fig. 2. Initial configurations of (a) zigzag (10,0) SWCNT, (b) armchair (10,10) SWCNT and (c) single polyethylene chain.

Table 1. Total number of atoms utilized in MD simulations.

	H atoms	C atoms	d (nm)	Length (nm)	θ°
Polyethylene (PE)	602	300	-	-	-
(10,0) SWCN	40	600	0.783	6.5541	0
(10,10) SWCN	60	600	1.356	4.1278	30

First, we use the limited-memory Broyden-Fletcher-Goldfarb-Shanno (LM-BFGS) minimization method [25] to relax the initial configurations of the polyethylene and the nanotubes to their local potential energy minimum. The iteration cycle is assumed to have converged if the gradient of the potential energy is less than or equal to 10^{-3}.Kcal/mol A°. Then we move the relaxed armchair SWCNT cell in close proximity to the relaxed polyethylene cell (such that the closest distance between the outer surface of nanotube and the nearest methylene monomer is 0.5 nm), and the composite system is enclosed in a computational box whose dimensions are approximately 5.25×2.87×3.59 nm. It is ensured that there are no overlapping positions between the SWCNT and polyethylene atoms. The LM-BFGS procedure is employed again to relax the composite system to its equilibrium. These procedures are repeated for the zigzag-polyethylene composite using different simulation box dimensions to accommodate different length of the (10,0) nanotube.

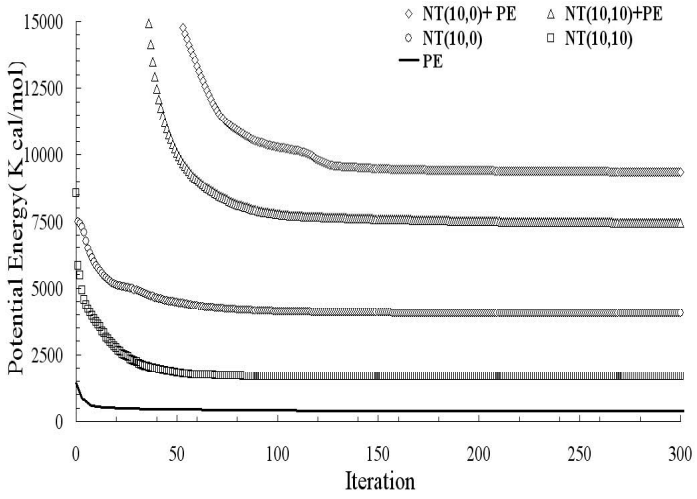

Fig. 3. Convergence of the minimization process for the potential energy of the individual constituents of the composites and the composites.

The minimal potential energies per atom of the relaxed configurations of (the polyethylene, the SWCNT and the nanocomposites) are shown in Fig. 3. As expected, the SWCNT have higher potential energy than the polyethylene chain due to the high level of energy of the predominant C-C bonding in the SWCNT compared to the lower energy of the C-H bonding in the polyethylene.

The evolution of the potential energy of four different composites is plotted in Fig. 4. The system could be reasonably assumed to have reached equilibrium as the change

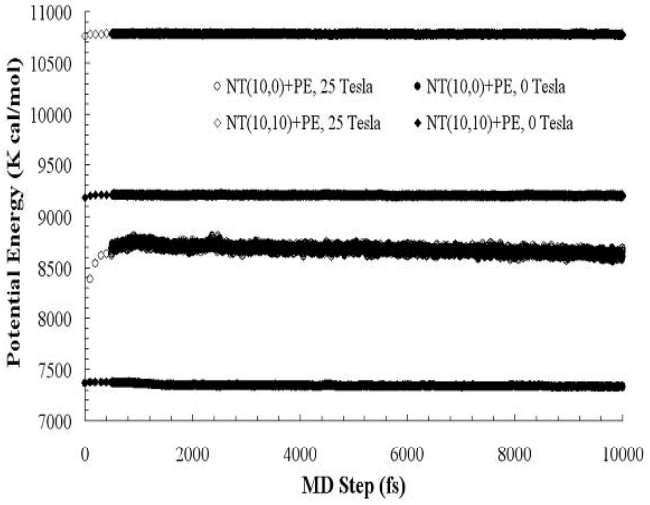

in potential energy over 10 pico second period is found to be within 0.1 % of the initial energy.

Fig. 4. Potential energy evolution for the armchair SWCNT-polyethylene and zigzag SWCNT-polyethylene composites

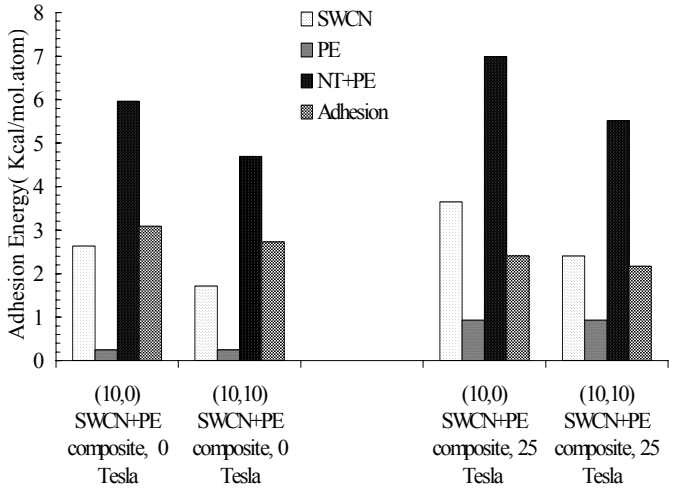

during 10 ps.

Fig. 5. Adhesion energy per atom between the SWCNT and the polyethylene chain.

For ease of comparison, the potential energies of the polyethylene chain, the two SWCNT and their corresponding composites are presented in Fig. 5. First, it is obvious that the chirality significantly influences the potential energy of both nanotubes and their corresponding composites, regardless of the magnetic field effect. As the chirality indices (chiral angle) increase, the potential energy decreases. This can be attributed to the effect of chirality of the SWCNT on its length and diameter. The SWCNT with low chirality indices tend to have smaller diameter and longer cylindrical axes compared to those with high chirality, such as the armchair nanotube (10,10). The correlation between the diameter of the SWCNT and the potential energy as obtained via molecular dynamics simulation conforms to that obtained by classical elasticity theory, where the total energies are inversely proportional to the square of the radius [26]. Therefore, the adhesion energy between the SWCNT and the polymer strongly depends on the diameter of SWCNT. Secondly, it is observed that the exposure to a 25 Tesla magnetic field increases the potential energies of the individual constituents comprising the two different composite systems and the composite systems themselves. Specifically, the magnetic annealing increases the potential energy of the zigzag SWCNT based composite by 17% and the armchair SWCNT based composite by 19%. Thirdly, it is found that the magnetic annealing decreases the adhesion energy by 23% and 20% for the zigzag SWCNT-polyethylene and armchair SWCNT –polyethylene composites, respectively. It can be explained away by the reorientation process and the final configurations of the composites assume under the 25 Tesla magnetic field shown in Figs. 6 and 7 and discussed below.

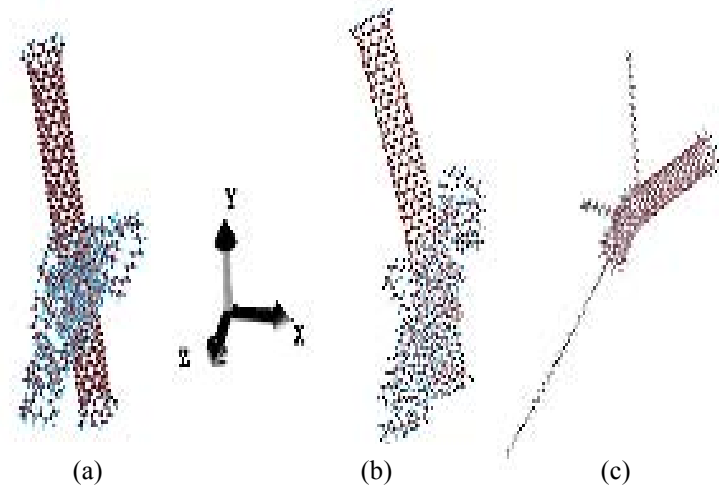

Fig. 6. Configurations of the zigzag SWCN-polyethylene (a) at 0 ps, (b) at 10 ps (no magnetic field), and (c) at 10 ps (25 Tesla magnetic field along the z-direction).

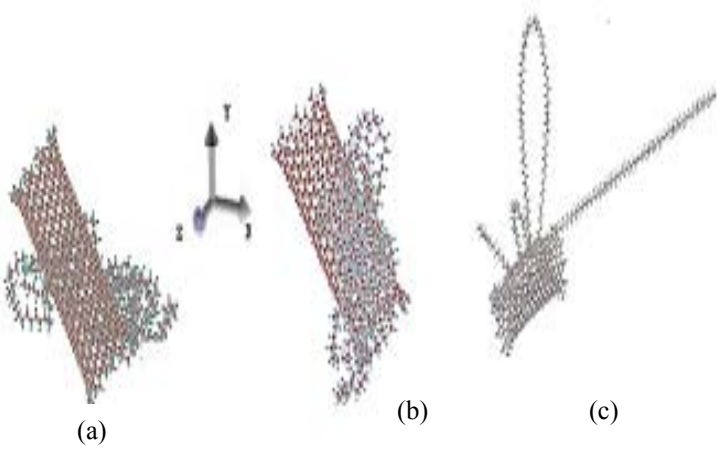

(a) (b) (c)

Fig. 7. Configurations of the armchair SWCN-polyethylene (a) at 0 ps, (b) at 10 ps (no magnetic field), and (c) at 10 ps (25 Tesla magnetic field along the z-direction)

The initial configuration for the zigzag SWCNT- polyethylene composite together with its final configurations with and without magnetic field is shown in Fig. 6. As the polyethylene chain is more susceptible to magnetic annealing than the zigzag SWCNT, it tries to reorient itself with the magnetic field fast and drags the zigzag SWCNT, which lags behind. In the process, debonding occurs between the polyethylene and the SWCNT leading to reduced adhesion energy.

Figure 7 shows the final configurations of the armchair SWCNT-polyethylene composite with and without magnetic annealing. It appears that the armchair SWCNT due to its paramagnetic axial susceptibility responds faster to the magnetic field, and as it moves, it pulls the diamagnetic polyethylene chain in the direction of the field. Again, this lead-lag motion causes debonding between the armchair SWCNT and the polyethylene chain, and reduces the over all adhesion energy of the nanocomposite. The details of the magnetic annealing of composites is discussed in Al-Haik and Hussaini [27].

CONCLUDING REMARKS

The present work based on the molecular dynamics simulations leads to the physical conclusions that i) the adhesion energy of a nanocomposite is a monotonic decreasing function of the chirality of the carbon nanotubes, ii) magnetic annealing increases the potential energy of the individual constituents as well the composite, and iii) adhesion energy suffers a significant decrease due to magnetic annealing although the trend of its dependence on chirality remains unaltered. With regard to the molecular dynamics simulations, it has been shown to be quite effective in investigating the interfacial mechanisms in nanocomposite, which are expensive if not hard to study in a laboratory; also, the Spreiter -Walter variant of the velocity Verlet algorithm is found to be efficient in that it circumvents the stringent explicit time-step restriction imposed by the Larmor frequency, particularly for high intensity magnetic field. In the final analysis, these computational results need to be validated by experimental observation.

REFERENCES

[1] Lordi, V., and Yao, N., 2000, ‘’Molecular Mechanics of Binding in Carbon Nanotube-Polymer Composites, ’’ J. Materials Research, 15, pp. 2770-2779.

[2] Choi, E.S., Brooks, J.S., Eaton, D.L., Al-Haik, M.S., Hussaini, M.Y., Garmestani, H., Li, D., and Dahmen, K., 2003, “Enhancement of Thermal and Electrical Properties of Carbon Nanotube Polymer Composites by Magnetic Field Processing,” J. Applied Physics, 94, pp. 6034-6039.

[3] Garmestani, H., Al-Haik, M.S., Dahmen, K., Tannenbaum, R., Li, D.S., Sablin, S.S., and Hussaini, M.Y., 2003, “ Polymer-Mediated Alignment of Carbon Nanotubes Under High Magnetic Fields,” Advanced Materials, 15, pp. 1918-1921.

[4] Qian, D., Dicky, E.C., Andrews, R., and Rantell, T., 2000, “ Load Transfer and Deformation Mechanisms in Carbon Nanotube-Polystyrene Composites,” Applied Physics Letters, 76, pp. 2868-2870.

[5] Wei, C., Cho, K., and Srivastava, D., 2001, “Chemical bonding of polymer carbon nanotube, ’’ MRS Spring Meeting Proceeding Paper.

[6] Liao, K., and Li, S., 2001,” Interfacial Characteristics of a Carbon Nanotube-Polystyrene Composite System,” Applied Physics Letters, 79, pp. 4225-4227.

[7] Frankland, S.J.V., Caglar, A., Brenner, D.W., and Griebel, M., 2002, “ Molecular Simulation of the Influence of Chemical Cross-Links on the Shear Strength of Carbon Nanotube-Polymer Interfaces,” J. Physical Chemistry B, 106, pp. 3046-3048.

[8] Frankland S.J.V., and Harik, V.M., 2003," Analysis of Carbon Nanotube Pull-Out From a Polymer Matrix," Surface Science, 52, p. L103-L108.

[9] Al-Haik, M., Hussaini, M.Y., and Garmestani, H., 2005," Adhesion Energy in Carbon Nanotube-Polyethylene Composite: Effect of Chirality," J. Applied Physics, 97, Paper No. 074306.

[10] Chang, B.H., Liu, Z.Q., Sun, L.F., Tang, D.S., Zhou, W.Y., Wang, G., Qian, L.X., Xie, S.S., Fen, J.H., and Wan, M.X., 2000, " Conductivity and Magnetic Susceptibility of Nanotube/ Polypyrrole Nanocomposites," J. Low Temperature Physics, 119, pp.41-48.

[11] Dresselhaus, M.S., Dresselhaus, G., and Saito, R., 1995, "Physics of Carbon Nanotubes," Carbon, 33, pp.883-891.

[12] Mensah, S.Y., Allotey, F.K.A., Mensah, N.G. and Nkrumah, G., 2001, " Differential Thermopower of a CNT Chiral Carbon Nanotube," J. Physics-Condensed Matter, 13, pp. 5653-5662.

[13] Liang, S.D., and Xu, N.S., 2003,"Chirality effect of single-wall carbon nanotubes on field emission," Applied Physics Letters, 83, pp. 1213-1215.

[14] Natsuki, T., Tantrakarn, K., and Endo, M., 2004, "Prediction of elastic properties for single-walled carbon nanotubes," Carbon, 42, pp.39-45.

[15] Leach, A.R., 2001, Molecular Modeling Principles and Applications, 2nd edition, Prentice Hall, Essex, England.

[16] Rizzo, R.C., and Jorgensen, W.L., 1999," OPLS All-Atom Model for Amines: Resolution of the Amine Hydration Problem," J. American Chemical Society, 121, pp.4827-4836.

[17] Lue, L., and Blankschtein, D., 1992, "Liquid-State Theory of Hydrocarbon Water-Systems - Application to Methane, Ethane and Propane," J. Physical Chemistry, 96, pp. 8582-8594.

[18] Jorgensen, W.L., Maxwell, D.S., and TiradoRives, J., 1996, "Development and Testing of the OPLS All-Atom Force Field on Conformational Energetics and Properties of Organic Liquids," J. American Chemical Society, 118, pp. 11225-11236.

[19] Kaminski, G., and Jorgensen, W.L., 1996, "Performance of the AMBER94, MMFF94, and OPLSAA force fields for modeling organic liquids," J. Physical Chemistry, 100, pp. 18010-18013.

[20] Weber T.A., and Annan N.D., 1982, " Molecular-Dynamics of Small Alkanes in An External Force-Field," Molecular Physics, 46, pp. 193-209.

[21] Tian, P., Bedrov, D., Smith, G.D., Glaser, M., and Maclennan, J.E., 2002,"A Molecular-Dynamics Simulation Study of the Switching Dynamics of a Nematic Liquid Crystal Under an Applied Electrical Field," J. Chemical Physics, 117, pp. 9452-9459.

[22] Spreiter, Q., and Walter, M., 1999, "Classical Molecular Dynamics Simulation with the Velocity Verlet Algorithm at Strong External Magnetic Fields," J. Computational Physics, 152, pp.102-119.

[23] Andersen, H.C., 1980, "Molecular Dynamics Simulations at Constant Pressure and-or Temperature," J. Chemical Physics, 72, pp. 2384-2393.

[24] Dudek, M.J., and Ponder, J.W., 1995, "Accurate Modeling of the Intramolecular Electrostatic Energy of Proteins," J. Computational Chemistry, 16, pp. 791-816.

[25] Zhu, C.Y., Byrd, R.H., Lu, P.H., and Nocedal, J., 1997,"Algorithm 778: L-BFGS-B: Fortran Subroutines for Large-Scale Bound-Constrained Optimization," ACM Transactions on Mathematical Software, 23, pp. 550-560.

[26] Gulseren, O., Yildirim, T., and Ciraci, S., 2002, " Systematic Ab-initio Study of Curvature Effects in Carbon Nanotubes," Physical Review B, 65, Art. No. 153405.

[27] Al-Haik, M.S., and Hussaini, M.Y., " Molecular Dynamics Simulation of Magnetic Field Induced Orientation of Nanotube -Polymer Composite," J. Applied Physics (in review).